3D Printed Effective Single-Mode Terahertz Antiresonant Hollow Core Fiber

SHUAI YANG[1], **XINZHI SHENG**[1], **GUOZHONG ZHAO**[2],
SHUQIN LOU[3], **AND JIAOYAN GUO**[2]

[1]School of Science, Beijing Jiaotong University, Beijing 100044, China
[2]Key Laboratory of Terahertz Optoelectronics, Ministry of Education, Department of Physics, Capital Normal University, Beijing 100048, China
[3]School of Electronic and Information Engineering, Beijing Jiaotong University, Beijing 100044, China

Corresponding authors: Xinzhi Sheng (xzhsheng@bjtu.edu.cn) and Guozhong Zhao (guozhong-zhao@126.com)

ABSTRACT An antiresonant hollow core effective single-mode terahertz fiber is proposed and successfully fabricated with a photosensitive resin (SomosEvoLVe 128) by a 3D printer. The single mode characteristics of the fiber are found to be related to the area of the semielliptical tubes in the cladding. By optimizing the cladding structure parameters, a Higher Order Mode Extinction Ratio (HOMER) of above 6 can be achieved. A 30 cm long sample with optimized structural parameters is obtained by cascading two 15 cm long fiber samples fabricated by a 3D printer. The transmission loss and the electric field distribution are measured by a terahertz time domain spectroscopy (TDS) system. The electric field distribution measured at the output end of the fiber sample has the Gaussian profile, which accords with single-mode field distribution. Experimental results show that the average loss is 0.048 cm^{-1} within the frequency range from 0.2 to 1 THz, and the minimum loss is obtained as low as 0.009 cm^{-1} at the frequency of 0.82 THz.

INDEX TERMS Optical waveguides, terahertz radiation, design optimization, 3D printing.

I. INTRODUCTION

The use of terahertz radiation (0.1–10 THz) is undergoing the rapidly growth since terahertz systems are now promising candidates for sensing, imaging, security, spectroscopy and communication [1]–[5]. To meet the demands of terahertz system integration, low loss and single-mode terahertz waveguides have attracted much attention in the recent years. In the early stages, numerous metallic terahertz waveguides were reported [6]–[8], including metal plates, metal tubes, and metal wires. Due to the high absorption loss of the metal to a terahertz wave and the difficulty for a terahertz wave to be coupled into metal waveguides, polymer waveguides have become more promising candidates with good flexibility and low absorption loss. In 2002, Han *et al.* reported the first plastic photonic crystal terahertz fiber with a high index core, exhibiting a low loss of 0.5 cm^{-1} within the frequency range of 0.1 to 3 THz [9]. Even so, the transmission loss of the terahertz waveguide is expected to be further reduced. In fact, the most transparent medium is dry air for terahertz waves, and hollow core fibers (HCFs) have also been shown to be

The associate editor coordinating the review of this manuscript and approving it for publication was Derek Abbott.

a solution for lowering the transmission loss. Based on the guidance mechanism, two types of HCFs are proposed. The first type of HCF is photonic bandgap (PBG) fiber, in which the light is guided inside the hollow core by PBG [10]–[12]. In 2008, Hassani *et al.* fabricated the first porous photonic bandgap Bragg fiber [10]. The total loss is lower than 0.057 cm^{-1}, but the bandwidth is less than 0.1 THz. In 2018, a PCF design based on hexagonal shaped holes incorporated within the core was proposed with a loss of only 0.029 cm^{-1} at 1.3 THz [12]. However, photonic band gap fibers generally have the disadvantages of narrow bandwidth and complex structure. The second type of HCF is an anti-resonant hollow core fiber (AR-HCF) [13]–[16], in which the light is guided by inhibited coupling between core mode and cladding mode. In 2008, Lu *et al.* proposed and fabricated the first Kagome hollow core terahertz fiber with a loss of less than 0.01 cm^{-1} [13]. In 2016, Lu, a member of our group, developed a new hollow core terahertz fiber with a tube-lattice cladding [14]. However, none of the terahertz waveguides above can effectively provide single-mode operation. Compared with multimode fibers, single-mode fibers can provide the advantages of low loss, low dispersion and low crosstalk for long-distance and large-capacity data transmission.

In recent years, hollow core single-mode terahertz fibers have been enthusiastically studied. Li *et al.* reported a flexible hollow core single-mode terahertz fiber with metamaterial cladding in 2016 [17], [18]. The fiber guides single TM mode within the frequency range from 0.31 and 0.44 THz, and its propagation loss was as low as 0.035 cm^{-1} within the single-mode window. With fabrication by digital light processing rapid prototyping, Hong *et al.* proposed a low loss asymptotically single-mode terahertz Bragg fiber in 2018 [19]; the fiber loss was less than 0.006 cm^{-1} over the frequencies of 0.246 to 0.276 THz, and the loss of the main competing mode HE$_{12}$ was at least ~4.3 times greater than that of the HE$_{11}$ mode. In addition, some designs of single-mode terahertz fibers have been reported [20]–[27], however, due to the difficulties in fabrication, only a few reported terahertz fibers have been fabricated [25], [27], and the rest of the designs only stay at the stage of theoretical analysis. With 3D printing technology maturing and its manufacturing accuracy continuously improving, an increasing number of terahertz hollow core fibers [28]–[33] have been fabricated with 3D printers. In 2019, we proposed and successfully fabricated a pentagram terahertz hollow core fiber and a birefringent terahertz fiber based on an elliptical hollow core with a 3D printer [32], [33]. Up to now most hollow core terahertz fibers fabricated with 3D printers are not single-mode terahertz waveguides, thus design and fabrication of single-mode terahertz waveguides is still an important issue in the scope of terahertz fibers by 3D printing technology.

In this paper, an effective single-mode terahertz AR-HCF is proposed. The cladding of the proposed fiber is composed of several semielliptical tubes. Compared with circular tubes, the cladding composed of elliptical tubes can provide better transmission characteristics and higher structural freedom [34]. When the cladding composed of semielliptical tubes, the fiber's transmission characteristics are almost the same as that of the elliptical tubes; but the size of the fiber is effectively reduced, which is more conducive to the miniaturization and integration of the terahertz system. Therefore, the fiber proposed in this paper is based on a cladding composed of the semielliptical tubes. The influence of the structural parameters on the fiber's single-mode characteristics is systematically studied. This study is conducive to the realization of single-mode operation of terahertz fibers with more diverse structures. The fiber samples with optimized parameters are fabricated by a 3D printer. The transmission loss and the single-mode characteristics of the samples are measured by a terahertz time domain spectroscopy (TDS) system.

II. FIBER DESIGN AND PARAMETER OPTIMIZATION

The cross-section of the proposed terahertz AR-HCF is shown in Fig. 1. The gray region is the photosensitive resin (SomosEvoLVe 128), which is a commonly used material for 3D printing. The refractive index of the photosensitive resin is 1.64+i0.04 at 0.6 THz, as measured in our previous
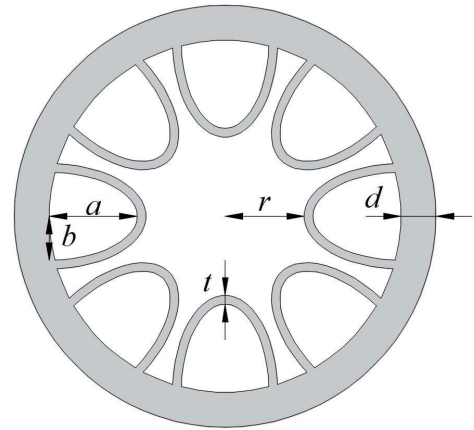

FIGURE 1. Cross-section of the proposed terahertz AR-HCF.

work [32]. The core radius of the proposed fiber is represented by r; the semi-major and semi-minor axes of the semielliptical tubes are represented by a and b, respectively; the wall thickness of the semielliptical tubes is represented by t, and the wall thickness of the outer circular tube, which works as a protective layer, is represented by d.

A finite-element method with PML boundary condition is used to perform the numerical calculations. The thickness of the PML set as 5 cm which is about three times the maximum wavelength. In the simulation process, the imaginary part of the complex refractive index of the material is brought into the calculation, so the obtained loss is the sum of the confinement loss and the material absorption. Considering the 3D printer's manufacturing accuracy, the fiber initial parameters are set as $r = 3$ mm, $a = 4.95$ mm, $b = 1.98$ mm, $t = 0.3$ mm and $d = 1$ mm. In this way, the other two important parameters can also be set. One is the semielliptical tubes' ellipticity $n_1 = 2.5$ (a/b), and another is the ratio of the major axis to the radius of the core $n_2 = 1.65$ (a/r). In the subsequent optimization process, the structural parameters are optimized by adjusting these two parameters (n_1 and n_2). The operating frequency is locked to 0.6 THz, which corresponds to the spectrum peak of the terahertz source of the TDS system used for experimental measurement, and the corresponding wavelength is 0.5 mm.

The electric field distributions and the loss spectra of the representative modes (HE$_{11}$, HE$_{21}$, TE$_{01}$ and TM$_{01}$) of 8 tube fiber are presented in Fig. 2. Single-mode fiber always refers to only the fundamental mode (HE$_{11}$) transmitted in the core, which is the lowest loss mode. Three second-order modes have similar circular electric field distributions, But their electric field vectors indicated by the arrow are different. TE$_{01}$ is the second lowest loss mode in most cases. Therefore, the loss ratio of TE$_{01}$ mode to HE$_{11}$ mode is regarded as the higher order mode extinction ratio (HOMER), which is an important parameter for evaluating the performance of the fiber's single-mode characteristics [35], [36]. Higher HOMER indicates high performance on single-mode characteristics. During simulation, the losses of different modes of the proposed terahertz fiber are calculated by the following
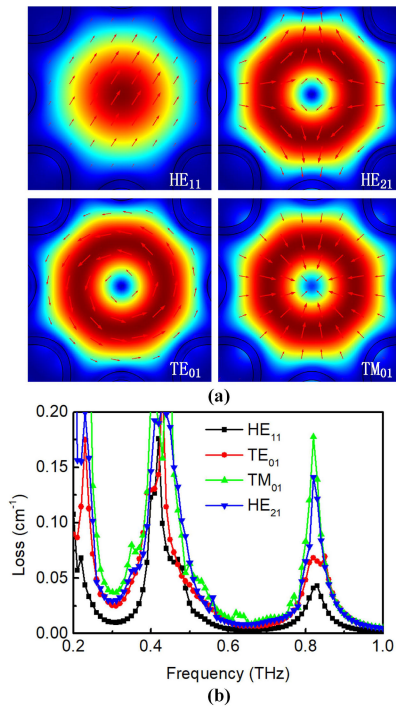
FIGURE 2. (a) Electric field distributions and (b) the loss spectra of the selected representative modes of 8 tubes fiber: HE_{11}, HE_{21}, TE_{01} and TM_{01}.

FIGURE 3. The distribution of HOMER, cross-sections and the distribution of the areas of semielliptical tube of the fiber with (a) 8 tubes, (b) 7 tubes and (c) 6 tubes.

equation [37]:

$$Loss = k_0 Im(n_{eff}) \qquad (1)$$

where k_0 is the wave vector in the vacuum and $Im(n_{eff})$ is the imaginary part of the effective refractive index.

First, the effect of tube number is considered on single mode characteristics of the fiber. The distribution of HOMER, cross-sections of the fiber and the distribution of the areas of semielliptical tubes of the fiber with 8 tubes, 7 tubes and 6 tubes are shown in Fig. 3(a-c). In the process of optimization, the core radius is fixed to 3 mm, and the two parameters n_1 and n_2 are optimized simultaneously by selecting multiple combinations based on the initial parameters of the fiber. For multiple combinations, the distribution of the HOMER shows a diagonal band-like distribution, and this distribution is similar to that of the area of the semielliptical cladding tube, as shown in Fig. 3. The change in the fibers' HOMER with the area of the semielliptical tubes is shown in Fig. 4.

As shown in Fig. 4, the HOMERs of the fibers with 6 tubes, 7 tubes and 8 tubes all show a peak, but the area corresponding to the peak is slightly shifted. The peak shift is attributed to the core shape will be slightly different and the effective refraction index corresponding to the TE_{01} mode will also be slightly different for the fiber with different cladding tubes. Among them, the fiber with 6 tubes shows a better performance for the HOMER than the fiber with 7 tubes or 8 tubes.

This phenomenon can be explained by the mode field distribution and core power ratio. The mode field distribution
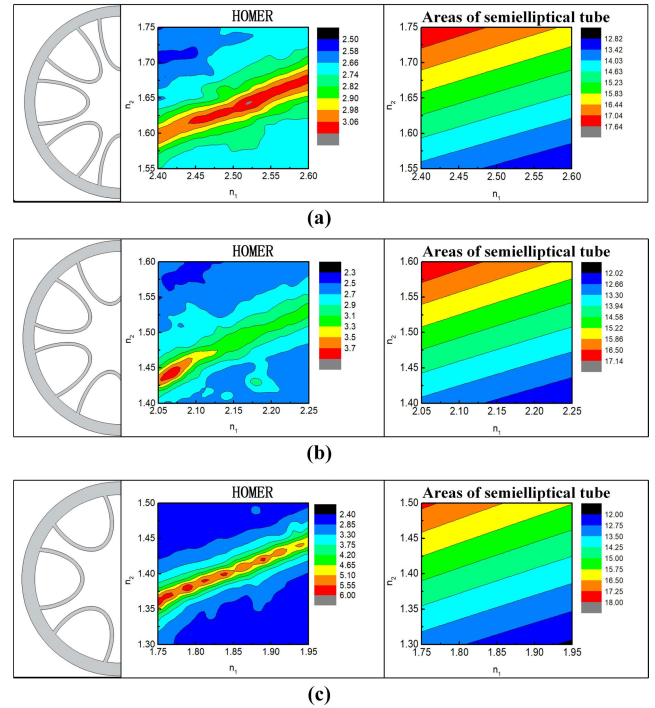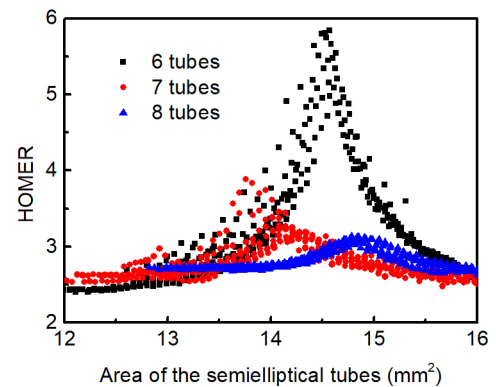

FIGURE 4. The HOMERs of the fiber with 6, 7, and 8 tubes as function of area of the semielliptical tube.

of TE_{01} mode for three structures with 6, 7 or 8 tubes at the frequency of 0.6 THz is shown in Fig. 5. It can be seen that there is more strongly coupling between TE_{01} mode and cladding mode for the structure with 6 tubes among three structures. This can also be also evaluated by the power ratio of core power to the total power of TE_{01} mode. For 6 tube structure, the core power only occupies 41.27%, which is lower than that of 7 tubes and 8 tubes structures. Therefore, the maximum HOMER can be obtained in the 6 tube structure.

The loss characteristics of the fibers with 6 tubes, 7 tubes and 8 tubes are also worthy of attention. The simulation results of loss in the frequency range from 0.2 to 1.2 THz are shown in Fig. 6. In the frequency range from 0.5 to 1.2 THz,
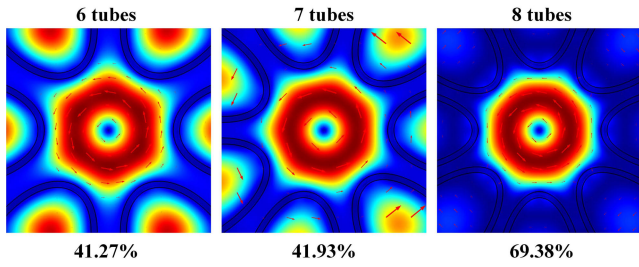
FIGURE 5. The mode field distribution of TE_{01} mode for three structures with 6, 7 or 8 tubes at the frequency of 0.6 THz.
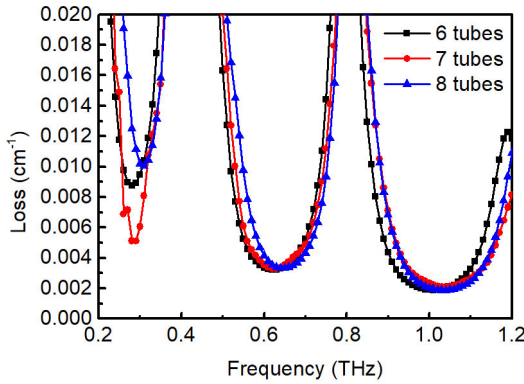

FIGURE 6. Loss spectra in the frequency range from 0.2 to 1.2 THz with 6, 7, and 8 tubes.

FIGURE 7. The effective refractive index of the cladding mode and TE_{01} mode as function of area of the semielliptical tube. And the electric field distribution of cladding mode and TE_{01} mode when coupling and uncoupling.

the 6 tubes and 8 tubes fibers provide lower losses than the 7 tubes fiber. The lowest loss of 6 tubes fiber is 0.0018 cm^{-1} at 1.01 THz, and that of 7 tubes and 8 tubes fiber is 0.0021 and 0.0018 cm^{-1} at 1.03 THz, respectively.

Because the 7 tubes structure is asymmetric, the HOMER data in Fig. 4 is more discrete than that of 6 tubes and 8 tubes structures. In the fiber loss spectrum shown in Fig. 6, the 7 tubes structure also shows a lower loss in the frequency range from 0.2 to 0.4 THz than that of the 6 tubes and 8 tubes structures. The reason for this phenomenon is the asymmetry of the 7 tubes structure that makes 7 tubes fiber has a large loss fluctuation in the low-frequency region.

Therefore, the fiber with 6 tubes is chosen as the basis for subsequent research, and then the area of the semielliptical tubes is considered to be the only factor that affects the fiber's single-mode characteristics.

The correlation between the area of the semielliptical tube and the fiber's single mode characteristics can be explained by the mode coupling of the cladding mode and TE_{01} mode. As shown in Fig. 7, as the area of the semielliptical tube increases, the effective refractive index (n_{eff}) of the cladding mode gradually increases. In contrast, the n_{eff} of the TE_{01} mode does not change substantially. Until the n_{eff} of the TE_{01} mode is close to that of the cladding mode, the two modes are severely coupled, which causes the loss to increase. After that, the n_{eff} of the cladding mode continues to increase and that of the TE_{01} mode tends to be stable again with the area of the semielliptical tube.
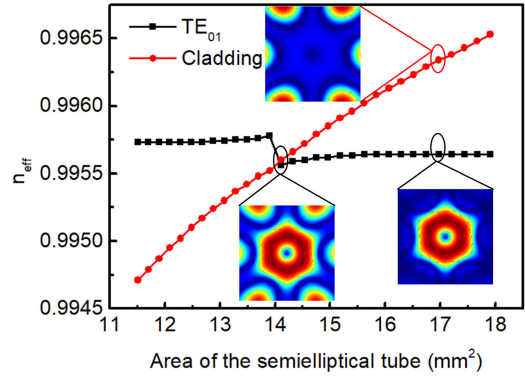
The effects of other factors on the fiber's single-mode characteristics are optimized as well, including the wall thickness of the semielliptical tubes and the core radius.

In the process of optimization, the wall thickness is selected to be 0.1 mm, 0.3 mm and 0.5 mm respectively. As the wall thickness increases, the losses of both the HE_{11} and TE_{01} modes both increase as shown in Fig. 8(a). When the wall thickness is different, the areas of the semielliptical tubes corresponding to the loss peaks of the TE_{01} mode are consistent with each other, and the loss of the HE_{11} mode hardly changes with the area of the elliptical tubes. Correspondingly, the peaks of the fiber HOMERs are consistent with each other, as shown in Fig. 8(b), in which a higher HOMER is obtained in the fiber with a thinner wall thickness. Considering the actual 3D printing fabrication limitations, a minimum wall thickness of 0.3 mm is chosen to make the wall thickness as thin as possible when the fiber sample is fabricated. The reported minimum wall thickness is approximately 0.3 mm.

Fig. 9 show the influence of the core radius on the HOMER as the core radius increases from 2.5 mm to 5 mm in steps of 0.5 mm for the fiber with different ellipticities of $n_1 = 1.7$, $n_1 = 1.8$ and $n_1 = 1.9$. All the HOMER distribution show a peak, but the corresponding elliptical tube area increases with the radius of the core.

The area of the semielliptical tube corresponding to the peak of the HOMERs shows a quadratic relationship with the core radius r, but a linear relationship with the square of the core radius (r^2) as shown in Fig. 10. It is worth noting that there are no significant differences in the relationship for semielliptical tubes with different ellipticities. On the other hand, the radius of the core also has an effect on the loss of the fiber [38]. The larger the core radius is, the lower the fiber loss. As the core radius increases, the losses of HE_{11} mode and TE_{01} mode both decrease. However, the loss of TE_{01} mode decreases faster than that of the HE_{11} mode, which leads to a decrease in the fiber's HOMER. Instead, when the core radius is decreased, the fiber's single mode characteristic is better, but the fiber loss is higher. After comprehensive consideration, the core radius is locked at 3.5 mm, under
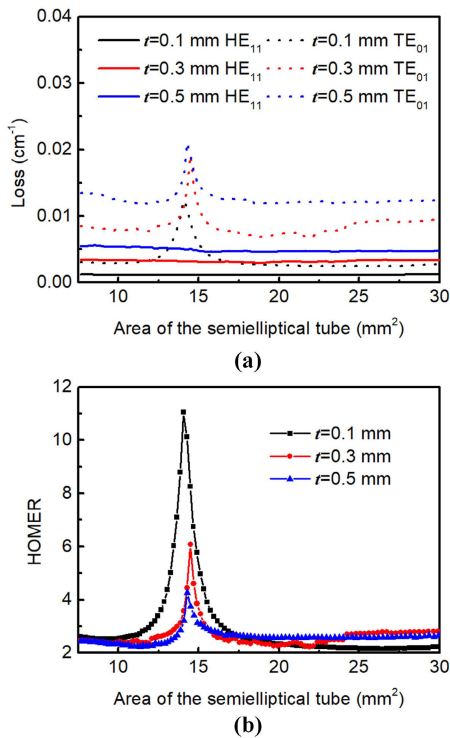
FIGURE 8. (a) Fiber loss of the HE_{11} and TE_{01} modes and (b) the HOMERs for different wall thicknesses as function of area of the semielliptical tube.

FIGURE 9. When the ellipticity is set to (a) $n_1 = 1.7$, (b) $n_1 = 1.8$ and (c) $n_1 = 1.9$, the HOMERs for different r as function of the semielliptical tube area.
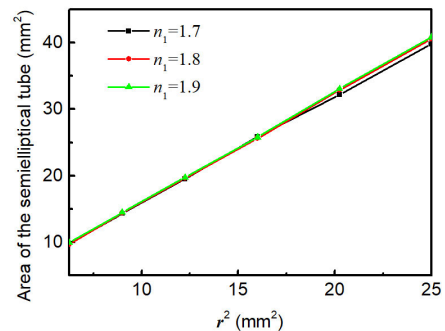
FIGURE 10. The optimal areas of semielliptical tube as function of the square of the core radius (r^2).
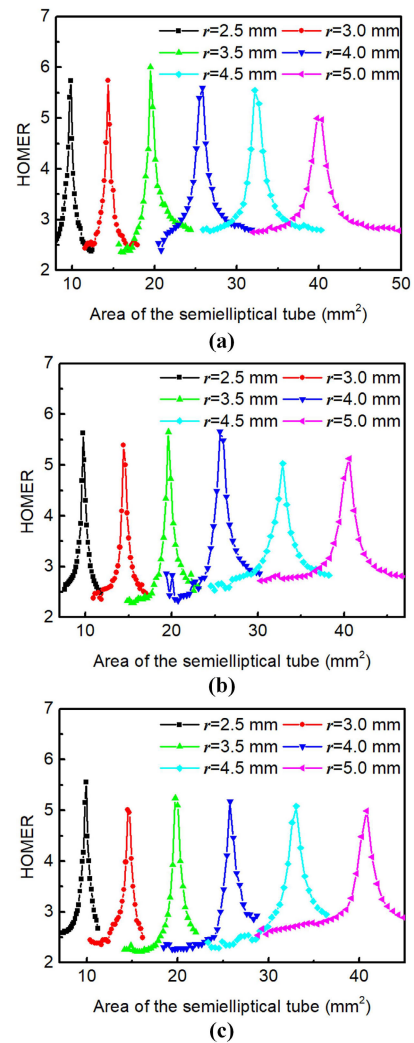
which the core radius corresponds to low loss and a maximum HOMER of 6.01 is obtained for the above simulation results.

According to the previous optimization results, the parameters of the fiber can be selected according to the following points. When the cladding consists of 6 semielliptical tubes, the single mode characteristics of the fiber are significantly better than those consisting of 7 or 8 semielliptical tubes. The wall thickness of the semielliptical tube should be as thin as possible within the feasibility of the fabrication. In this paper, the accuracy of the 3D printer is taken into consideration. The two parameters n_1 and n_2 both affect the area of the semielliptical tubes. The selected set of data for the single model performance in the optimization results is $n_1 = 1.7$ and $n_2 = 1.34$.

Based on the optimized parameters, the loss of HE_{11} and TE_{01} mode in the frequency range of 0.2 to 1 THz are shown in Fig. 11(a). The loss spectrum is divided into three transmission windows by two resonant peaks. The simulation results show that the lowest loss of HE_{11} mode is obtained at 0.62 THz, which is 0.0029 cm^{-1}. The resonant frequency can be also predicted well by the anti-resonant reflecting optical waveguide (ARROW) model [39] and estimated by the equation:

$$f = \frac{mc}{2t\sqrt{n^2-1}} \qquad (2)$$

where t is the wall thickness, n is the material refractive index, and m is an integer. In the non-resonant region, a higher HOMER can be obtained., The HOMER is higher than 6 at
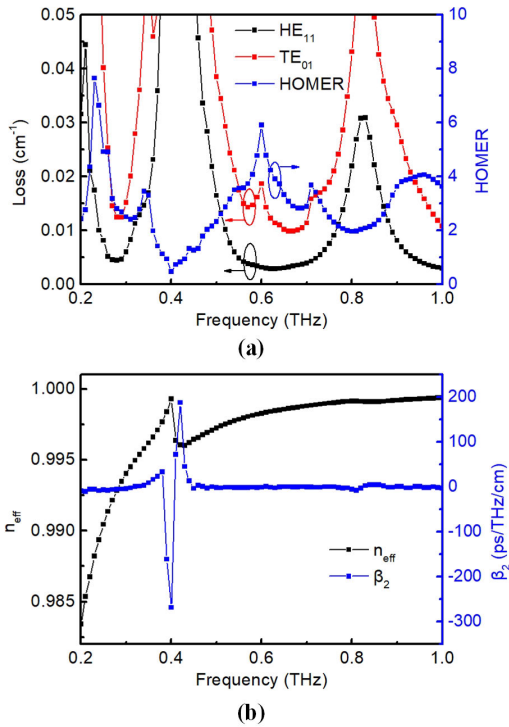
the operating frequency of 0.6 THz. At the resonance frequency, due to energy leakage in both modes, the HOMER is significantly reduced.

The effective refractive index and dispersion of HE_{11} mode are shown in Fig. 11(b). The dispersion (β_2) can be

FIGURE 11. (a) Simulation loss of the HE_{11} mode, TE_{01} mode and HOMER with optimized parameters. (b) The effective refractive index and dispersion of HE_{11} mode as function of frequency.

FIGURE 12. The loss as function of the frequency by using ZEONEX and SomosEvoLVe 128 materials, respectively.

FIGURE 13. Simulation loss of the HE_{11} and TE_{01} modes and HOMER of the fiber as function of bending radius.
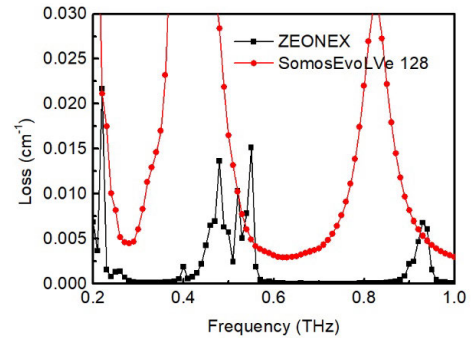
calculated by [40]:

$$\beta_2 = \frac{\omega}{c}\frac{\partial^2 n_{\text{eff}}}{\partial \omega^2} + \frac{2}{c}\frac{\partial n_{\text{eff}}}{\partial \omega} \qquad (3)$$
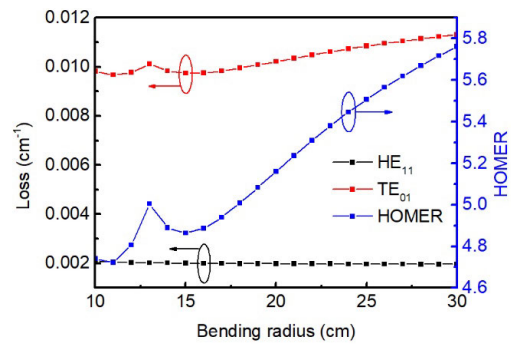
where ω is the angular frequency. The effective refractive index increases smoothly as the frequency increases and approaches 1 except a sudden change at the resonance frequencies due to energy leakage. The proposed fiber has a flat dispersion of less than 3 ps/THz/cm in the non-resonant region, and suddenly changes at the resonant frequency.

In summary, the fiber with 6 semielliptical tubes is more conducive to obtaining good single mode characteristics. The optimization results show that the thin wall thickness is helpful to obtain low loss and high HOMER. But the thinner the wall thickness is, the more difficult it is to be fabricated. The larger the core radius is, the lower the loss of HE_{11} and TE_{01} modes is, thereby the HOMER will decrease accordingly.

Using materials with low absorption coefficients is beneficial for obtaining lower losses and higher HOMER. The simulation fiber loss as function of the frequency for using ZEONEX and SomosEvoLVe 128 materials is shown in Fig.12. When ZEONEX is used as material whose refractive index is $1.52+i5.7 \times 10^{-4}$ at 0.6 THz, the fiber loss is only 8.6×10^{-5} cm^{-1} at the operating frequency (0.6 THz), which is 36 times lower than that of SomosEvoLVe 128. And the HOMER can be improved to 9.07 for ZEONEX.

Apart from Zeonex, high resistive silicon also has very low loss in terahertz regime for terahertz hollow core fiber designs [41], [42].

The influence of bending on fiber loss and single mode characteristic is also concerned. Bending loss can be simulated by replacing the bent fiber with a straight one which has an equivalent index distribution [37], [43]:

$$n(x, y) = n0(x, y)(1 + \frac{x\sin\theta + y\cos\theta}{R_{\text{bend}}}) \qquad (4)$$

where $n_0(x,y)$ is the initial refractive index distribution of the fiber, R_{bend} is the bending radius of the fiber, and θ is the angle between the bending direction and the y axis. When the bending radius increases from 10 cm to 30 cm, and the bending direction is along the y axis, the losses of the HE_{11} and TE_{01} modes and HOMER of the fiber are shown in the Fig. 13.

It can be seen from Fig. 13 that the loss of TE_{01} mode gradually increases with the increase of the bending radius, while the loss of HE_{11} does not change significantly, resulting in an increase in the HOMER. This is because when the bending radius is smaller, the refractive index of the inner wall changes more, and the TE_{01} mode couples with the cladding modes in several semielliptical tubes instead of all six semielliptical tubes. Even if the bending radius is reduced to 10 cm, the fiber can still obtain a HOMER of 4.7. At this time, the bending radius is close to the limit, which is about 5 times fiber diameter.
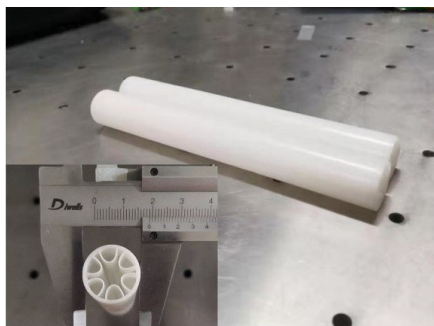
FIGURE 14. The fiber samples fabricated by the 3D printer.

FIGURE 15. Total loss of 30 cm long samples with two different cascade methods measured by the terahertz TDS experimentally.

III. EXPERIMENTAL RESULTS AND DISCUSSION

The fiber samples are measured by a homemade terahertz time-domain spectrometer. The laser produces 800 nm wavelength pulses of 100 fs duration with an 82 MHz repetition rate. The light beam is split into two linear polarized beams by using a polarization beam splitter (PBS), where one is used as the pump beam and another as the probe beam. The delay line consists of a motorized stage to scan the delay time of the terahertz pulse. The waveform of terahertz pulse is measured by detecting differential current as a function of delay time.

Two 15 cm long fiber samples are fabricated with a photosensitive resin (SomosEvoLVe 128) by a 3D printer, and the corresponding cross section is shown in Fig. 14. The core radius of the sample $r = 3.5$ mm, the wall thickness of the outer circular tube $d = 1$ mm, $n_1 = 1.7$, and $n_2 = 1.34$. The wall thickness of the semielliptical tube $t = 0.39$ mm, which is almost the minimum for the 3D printer fabrication capacity. And the outer diameter of the fiber sample is 19 mm. Since it is difficult for 3D printers to fabricate long sample, a 30 cm long fiber sample is fabricated by cascading the two 15 cm long fiber samples.

To ensure that the amount of input coupled light is similar for all experiments, the fiber samples are held in the setup using a metal baffle with an aperture in the center corresponding to the size of the samples. A 3 cm long sample is used as a reference which acts like an aperture stop. The detector is a differential photodiode used to detect the intensity difference between the two polarization probe beams produced by the polarization beam splitter (PBS). To restrain the noise, the emitter bias voltage is modulated with a low-frequency square signal, and the receiver's output is amplified with a lock-in amplifier. The fiber loss or attenuation constant is obtained in the experiment by the equation [44]:

$$\alpha = \frac{2 \ln(A_{\text{sam}}/A_{\text{ref}})}{L} \qquad (5)$$

where A_{ref} and A_{sam} indicate the terahertz amplitude of the reference and sample respectively, and L indicates the length difference between reference and sample.

The 30 cm long samples are obtained by direct cascade and cascade after rotation of 30 degrees, respectively. The cascading method after rotating 30 degrees is the most serious situation of cladding dislocation. These two cascade methods
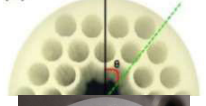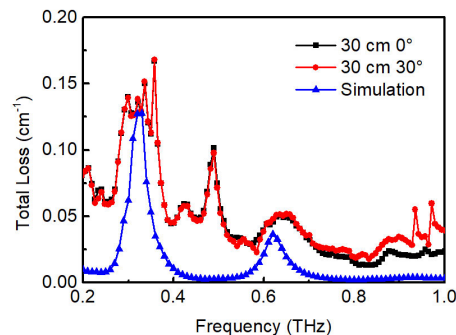
are called as perfect cascade and dislocation cascade, respectively. The losses of the 30 cm long samples with two different cascade methods are measured by the terahertz TDS, and measurement result are shown in Fig. 15. In the case of perfect cascade, the loss is slightly lower than that of dislocation cascade. But the loss difference with two different cascading methods is not obvious. This is because the fiber proposed in this paper confines most of the terahertz waves in the core and there is almost no leakage to the cladding. Therefore, the dislocation of the cladding has little effect on the loss. The perfectly cascaded 30 cm long sample can provide an average loss of 0.048 cm^{-1} in the frequency range from 0.2 to 1 THz, and the minimum loss obtained is 0.009 cm^{-1} at 0.82 THz that is three orders of magnitude lower than that of the bulk material (10.05 cm^{-1}). The additional loss peak around 0.5 THz may be caused by the anti-crossing between fundamental mode and HOMs [27] or the sample fabrication process deviation.

Electric field distribution is an important basis for proving the fiber single-mode operation. Therefore, the electric field distribution is measured by the single-sided method. The metal plate fixed on the displacement platform is placed at the fiber output end. With 0.25 mm movement per step of the displacement platform, the metal plate gradually blocks the signals at the output end of the fiber. The change between the terahertz amplitudes measured after and before each step is the electric field intensity in this step. Using the above method, the normalized electric field distribution at the output end of the perfectly cascaded 30 cm long sample is restored as shown in Fig. 16. The electric field distribution shown in Fig. 16 is similar to that of the HE_{11} mode with a Gaussian distribution. This means the fiber is effective single-mode operation.

In fact, 15 cm long samples are also measured. However, there is a significant gap between the measurement results and the simulation results. The reasons for this phenomenon can be explained that the measured total loss by the experiment consists of the fiber's transmission loss and the coupling loss including the input coupling loss from the terahertz source to input end of the fiber and output coupling loss from output end of the fiber to the detector. In the experimental system mentioned above, the distance for placing the sample

TABLE 1. The comparison of the fabricated terahertz fibers being reported.

| FIBER MODEL	MATERIAL	OPERATING FREQUENCY	CORE DIAMETER	OUTER DIAMETER	SIMULATED LOSS	EXPERIMENTAL LOSS	REF
	TEFLON	0.77 THz	5.5 mm		5×10^{-4} cm^{-1}	2×10^{-3} cm^{-1}	[13]
	ZEONEX	0.1-1.5 THz	3.3-4 mm		5.7×10^{-3} cm^{-1}	5.7×10^{-3} cm^{-1}	[14]
	PP	2.1 THz	1.3 mm	4.5mm		7.9×10^{-3} cm^{-1}	[16]
	ENVISIONTEC HTM140	0.265 THz	9.484 mm	45.9mm		3.3×10^{-3} cm^{-1}	[19]
	VEROWHITEPLUS	0.75 THz	9mm			2×10^{-3} cm^{-1}	[28]
	PHOTOSENSITIVE RESIN	0.6 THz	7 mm	19 mm	2.9×10^{-3} cm^{-1}	9×10^{-3} cm^{-1}	This paper
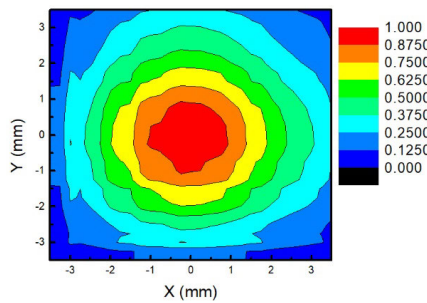
FIGURE 16. The normalized electric field distribution at the output end of the perfectly cascaded 30 cm long sample.

is fixed at 40 cm, and this distance cannot be changed. Compared with a 30 cm long sample, a 15 cm long sample needs to transmit a longer distance in free space from the output end of the fiber to terahertz detector. At this time, the influence of the divergence angle has to be considered.

The normalized electric field distribution at the output end of the 15 cm long sample and that near the detector (12.5 cm away from the output end) are measured respectively as shown in Fig. 17 (a) and (b). The label X on the coordinate axis is the displacement distance of the metal plate. By comparing the electric field distribution in Fig. 17 (a) and (b), it can be found that after 12.5 cm of free space transmission, the diameter of the spot has increased from 7 mm to 18 mm due to the divergence angle. Part of the energy is beyond the range that the detector can receive, leading to a significant increase in the coupling loss for the case of 15 cm

long sample. For the 30 cm long sample, its output end is already very close to the detector. Therefore, the coupling loss induced by the divergence angle has little effect on measured loss. Since the output coupling loss caused by the divergence angle is difficult to be accurately measured under the current experimental conditions, the effect of the divergence angle can only be reduced by making the sample length closer to the sample placement space in the experiment. In addition, the influence of higher-order modes (HOMs) may also cause this phenomenon. The transmission distance of 15 cm is too short that the mode coupling in the fiber has not been completed.

A comparison of the reported terahertz fibers that has been fabricated is shown in Table 1. Among these fibers listed, their materials, operating frequency and core diameter are different, and these parameters have obvious effects on fiber loss. Under normal circumstances, the larger core diameter and higher operating frequency make the transmission loss lower. Materials with lower absorption coefficients can also contribute to lower the transmission losses further. Although the absorption coefficient of photosensitive resin used as fiber material in our experiment is two orders of magnitude higher than that of ZEONEX recognized as a transparent material in the terahertz band, the measured loss of the proposed fiber in this paper is in the same order of magnitude with terahertz fiber with low absorption ZEONEX material. Photosensitive resin is the most commonly used and cheap material for 3D printer and thus the cost of the proposed fiber is very lower. If the proposed fiber structure uses ZEONEX as the material,
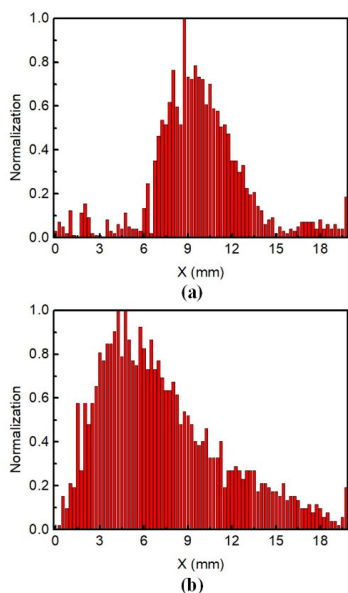
FIGURE 17. The normalized electric field distribution (a) at the output end of the 15 cm long sample and (b) that near the detector (12.5 cm away from the output end of the 15 cm long sample).

simulation loss can be reduced by at least one order of magnitude as shown in Fig.12. This result proves the proposed fiber structure is very efficient for lowering fiber loss.

IV. CONCLUSION

In this paper, an effective single-mode AR-HCF is proposed and fabricated with a photosensitive resin (SomosEvoLVe 128) by a 3D printer. Its cladding structure consists of several semielliptical tubes. Simulation results show that the fiber's HOMER is related to the area of the semielliptical tube. The optimal area of the semielliptical tube varies linearly with the square of the core radius. The 30 cm long sample is constructed by cascading the two 15 cm long fiber samples fabricated by a 3D printer. The 30 cm long samples with two different cascade methods are measured by a terahertz TDS. The electric field distribution at the output end of the fiber sample is measured and match the Gaussian distribution of the fundamental mode, which verifies the fiber's single-mode characteristics. Experimental results show that the average loss is 0.048 cm^{-1} within the frequency range from 0.2 to 1 THz, and the minimum loss is 0.009 cm^{-1} at 0.82 THz. The measured loss is slightly higher than simulation loss due to the coupling loss.

REFERENCES

[1] X. Yang, T. Wu, L. Zhang, D. Yang, N. Wang, B. Song, and X. Gao, "CNN with spatio-temporal information for fast suspicious object detection and recognition in THz security images," *Signal Process.*, vol. 160, pp. 202–214, Jul. 2019.

[2] A. Afroozeh, K. Innate, J. Ali, and P. P. Yupapin, "THz frequency generation using Gaussian pulse for medical applications," *Optik*, vol. 124, no. 5, pp. 416–419, Mar. 2013.

[3] K. I. Zaytsev, K. G. Kudrin, S. A. Koroleva, I. N. Fokina, S. I. Volodarskaya, E. V. Novitskaya, A. N. Perov, V. E. Karasik, and S. O. Yurchenko, "Medical diagnostics using terahertz pulsed spectroscopy," *J. Phys., Conf. Ser.*, vol. 486, Mar. 2014, Art. no. 012014.

[4] C. S. Mishra, A. Nayyar, G. Suseendran, and G. Palai, "L-shape Si-waveguide for THz-communication," *Optik*, vol. 178, pp. 509–512, Feb. 2019.

[5] N. Khalid, N. A. Abbasi, and O. B. Akan, "Statistical characterization and analysis of low-THz communication channel for 5G Internet of Things," *Nano Commun. Netw.*, vol. 22, Dec. 2019, Art. no. 100258.

[6] R. Mendis and D. Grischkowsky, "Undistorted guided-wave propagation of subpicosecond terahertz pulses," *Opt. Lett.*, vol. 26, no. 11, pp. 846–848, 2001.

[7] G. Gallot, S. P. Jamison, R. W. McGowan, and D. Grischkowsky, "Terahertz waveguides," *J. Opt. Soc. Amer. B*, vol. 17, no. 5, pp. 851–863, May 2000.

[8] K. Wang and D. M. Mittleman, "Metal wires for terahertz wave guiding," *Nature*, vol. 432, no. 7015, pp. 376–379, Nov. 2004.

[9] H. Han, H. Park, M. Cho, and J. Kim, "Terahertz pulse propagation in a plastic photonic crystal fiber," *Appl. Phys. Lett.*, vol. 80, no. 15, pp. 2634–2636, Apr. 2002.

[10] A. Hassani, A. Dupuis, and M. Skorobogatiy, "Porous polymer fibers for low-loss terahertz guiding," *Opt. Exp.*, vol. 16, no. 9, pp. 6340–6351, 2008.

[11] J. Fan, Y. Li, M. Hu, L. Chai, and C. Wang, "Design of broadband porous-core bandgap terahertz fibers," *IEEE Photon. Technol. Lett.*, vol. 28, no. 10, pp. 1096–1099, May 15, 2016.

[12] S. Rana, A. S. Rakin, M. R. Hasan, M. S. Reza, R. Leonhardt, D. Abbott, and H. Subbaraman, "Low loss and flat dispersion Kagome photonic crystal fiber in the terahertz regime," *Opt. Commun.*, vol. 410, pp. 452–456, Mar. 2018.

[13] J.-Y. Lu, C.-P. Yu, H.-C. Chang, H.-W. Chen, Y.-T. Li, C.-L. Pan, and C.-K. Sun, "Terahertz air-core microstructure fiber," *Appl. Phys. Lett.*, vol. 92, no. 6, Feb. 2008, Art. no. 064105.

[14] W. Lu, S. Lou, and A. Argyros, "Investigation of flexible low-loss hollow-core fibres with tube-lattice cladding for terahertz radiation," *IEEE J. Sel. Topics Quantum Electron.*, vol. 22, no. 2, pp. 214–220, Mar. 2016.

[15] G. K. M. Hasanuzzaman, S. Iezekiel, C. Markos, and M. S. Habib, "Hollow-core fiber with nested anti-resonant tubes for low-loss THz guidance," *Opt. Commun.*, vol. 426, pp. 477–482, Nov. 2018.

[16] M. M. Nazarov, A. V. Shilov, K. A. Bzheumikhov, Z. C. Margushev, V. I. Sokolov, A. B. Sotsky, and A. P. Shkurinov, "Eight-capillary cladding THz waveguide with low propagation losses and dispersion," *IEEE Trans. THz Sci. Technol.*, vol. 8, no. 2, pp. 183–191, Mar. 2018.

[17] H. Li, G. Ren, S. Atakaramians, B. T. Kuhlmey, and S. Jian, "Linearly polarized single TM mode terahertz waveguide," *Opt. Lett.*, vol. 41, no. 17, pp. 4004–4007, Sep. 2016.

[18] H. Li, S. Atakaramians, R. Lwin, X. Tang, Z. Yu, A. Argyros, and B. T. Kuhlmey, "Flexible single-mode hollow-core terahertz fiber with metamaterial cladding," *Optica*, vol. 3, no. 9, pp. 941–947, Sep. 2016.

[19] B. Hong, M. Swithenbank, N. Greenall, R. G. Clarke, N. Chudpooti, P. Akkaraekthalin, N. Somjit, J. E. Cunningham, and I. D. Robertson, "Low-loss asymptotically single-mode THz Bragg fiber fabricated by digital light processing rapid prototyping," *IEEE Trans. THz Sci. Technol.*, vol. 8, no. 1, pp. 90–99, Jan. 2018.

[20] K. Ahmed, S. Chowdhury, B. K. Paul, M. S. Islam, S. Sen, M. I. Islam, and S. Asaduzzaman, "Ultrahigh birefringence, ultralow material loss porous core single-mode fiber for terahertz wave guidance," *Appl. Opt.*, vol. 56, no. 12, pp. 3477–3483, 2017.

[21] J. Luo, S. Chen, H. Qu, Z. Su, L. Li, and F. Tian, "Highly birefringent single-mode suspended-core fiber in terahertz regime," *J. Lightw. Technol.*, vol. 36, no. 16, pp. 3242–3248, Aug. 15, 2018.

[22] S. Sen, M. S. Islam, B. K. Paul, M. I. Islam, S. Chowdhury, K. Ahmed, M. R. Hasan, M. S. Uddin, and S. Asaduzzaman, "Ultra-low loss with single mode polymer-based photonic crystal fiber for THz waveguide," *J. Opt. Commun.*, vol. 40, no. 4, pp. 411–417, Oct. 2019.

[23] M. A. Habib and M. S. Anower, "Design and numerical analysis of highly birefringent single mode fiber in THz regime," *Opt. Fiber Technol.*, vol. 47, pp. 197–203, Jan. 2019.

[24] C. Wei, R. J. Weiblen, C. R. Menyuk, and J. Hu, "Negative curvature fibers," *Adv. Opt. Photonics.*, vol. 9, no. 3, pp. 504–561, 2017.

[25] P. Uebel, M. C. Günendi, M. H. Frosz, G. Ahmed, N. N. Edavalath, J.-M. Ménard, and P. S. J. Russell, "Broadband robustly single-mode hollow-core PCF by resonant filtering of higher-order modes," *Opt. Lett.*, vol. 41, no. 9, pp. 1961–1964, 2016.

[26] J. Sultana, M. S. Islam, C. M. B. Cordeiro, M. S. Habib, A. Dinovitser, B. W.-H. Ng, and D. Abbott, "Exploring low loss and single mode in antiresonant tube lattice terahertz fibers," *IEEE Access*, vol. 8, pp. 113309–113317, 2020.

[27] J. Sultana, M. S. Islam, C. M. B. Cordeiro, M. S. Habib, M. Kaushik, A. Dinovitser, B. W.-H. Ng, H. Ebendorff-Heidepriem, and D. Abbott, "Hollow core inhibited coupled antiresonant terahertz fiber: A numerical and experimental study," *IEEE Trans. THz Sci. Technol.*, early access, Oct. 16, 2020, doi: 10.1109/TTHZ.2020.3031727.

[28] J. Yang, J. Zhao, C. Gong, H. Tian, L. Sun, P. Chen, L. Lin, and W. Liu, "3D printed low-loss THz waveguide based on Kagome photonic crystal structure," *Opt. Exp.*, vol. 24, no. 20, pp. 22454–22460, Oct. 2016.

[29] P. Van, J. Gorecki, F. Numkam, V. Apostolopoulos, and F. Poletti, "3D-printed polymer antiresonant waveguides for short-reach terahertz applications," *Appl. Opt.*, vol. 57, no. 14, pp. 3953–3958, 2018.

[30] A. Cruz, C. Cordeiro, and M. Franco, "3D printed hollow-core terahertz fibers," *Fibers*, vol. 6, no. 3, Jun. 2018, Art. no. 43.

[31] S. Li, Z. Dai, Z. Wang, P. Qi, Q. Su, X. Gao, C. Gong, and W. Liu, "A 0.1 THz low-loss 3D printed hollow waveguide," *Optik*, vol. 176, pp. 611–616, Jan. 2019.

[32] S. Yang, X. Sheng, G. Zhao, Y. Wang, and Y. Yu, "Novel pentagram THz hollow core anti-resonant fiber using a 3D printer," *J. Infr., Millim., THz Waves*, vol. 40, no. 7, pp. 720–730, Jul. 2019.

[33] S. Yang, X. Sheng, G. Zhao, and S. Li, "Simple birefringent terahertz fiber based on elliptical hollow core," *Opt. Fiber Technol.*, vol. 53, Dec. 2019, Art. no. 102064.

[34] M. S. Habib, O. Bang, and M. Bache, "Low-loss single-mode hollow-core fiber with anisotropic anti-resonant elements," *Opt. Exp.*, vol. 24, no. 8, pp. 8429–8436, 2016.

[35] F. Poletti, "Nested antiresonant nodeless hollow core fiber," *Opt. Exp.*, vol. 22, no. 20, pp. 23807–23828, 2014.

[36] M. S. Habib, J. E. Antonio-Lopez, C. Markos, A. Schülzgen, and R. Amezcua-Correa, "Single-mode, low loss hollow-core anti-resonant fiber designs," *Opt. Exp.*, vol. 27, no. 14, pp. 3824–3836, 2019.

[37] X. Wang, S. Lou, and W. Lu, "Bend-resistant large-mode-area photonic crystal fiber with a triangular-core," *Appl. Opt.*, vol. 52, no. 18, pp. 4323–4328, 2013.

[38] E. A. J. Marcatili and R. A. Schmeltzer, "Hollow metallic and dielectric waveguides for long distance optical transmission and lasers," *Bell Syst. Tech. J.*, vol. 43, no. 4, pp. 1783–1809, Jul. 1964.

[39] H. P. Uranus, H. J. W. M. Hoekstra, and E. van Groesen, "Considerations on material composition for low-loss hollow-core integrated optical waveguides," *Opt. Commun.*, vol. 260, no. 2, pp. 577–582, Apr. 2006.

[40] I. M. Saiful, J. Sultana, A. Dinovitser, M. Faisal, M. R. Islam, B. H. Ng, and D. Abbott, "Zeonex-based asymmetrical terahertz photonic crystal fiber for multichannel communication and polarization maintaining applications," *Appl. Opt.*, vol. 57, no. 4, pp. 666–672, 2018.

[41] M. A. Islam, M. R. Islam, M. M. I. Khan, J. A. Chowdhury, F. Mehjabin, and M. Islam, "Highly birefringent slotted core photonic crystal fiber for THz wave propagation," *Phys. Wave Phenomena*, vol. 28, no. 1, pp. 58–67, Jan. 2020.

[42] T. Yang, C. Ding, R. W. Ziolkowski, and Y. J. Guo, "Circular hole ENZ photonic crystal fibers exhibit high birefringence," *Opt. Exp.*, vol. 26, no. 13, pp. 17264–17278, 2018.

[43] Y. Tsuchida, K. Saitoh, and M. Koshiba, "Design and characterization of single-mode holey fibers with low bending losses," *Opt. Exp.*, vol. 13, no. 12, pp. 4770–4779, 2005.

[44] J. Chen, Y. Chen, H. Zhao, G. J. Bastiaans, and X. C. Zhang, "Absorption coefficients of selected explosives and related compounds in the range of 0.1-2.8 THz," *Opt. Exp.*, vol. 15, no. 19, pp. 12060–12067, 2007.

XINZHI SHENG is currently a full-time Professor with the School of Science, Beijing Jiaotong University, Beijing, China. He has authored or coauthored more than 80 journal articles and conference papers. He holds more than 20 authorized patents. His current research interests include optical fiber communication, fiber sensing, and fiber devices.

GUOZHONG ZHAO was born in Inner Mongolia, in 1964. He graduated from the Department of Physics, Inner Mongolia University, in 1989, and received the Ph.D. degree from the Institute of Physics, Chinese Academy of Sciences.

He investigated the nonlinear optical properties and optical bistability of semiconductor superlattices during his Ph.D. degree. In 1996, he joined Beijing Jiaotong University as a Lecturer. He worked on nonlinear optics and ultrafast optics and became an Associate Professor, in October 1997. In September 2000, he joined the European Program TERAVISION (IST-1999-10154), as a Postdoctoral Researcher at the Delft University of Technology, The Netherlands, where he studied the terahertz wave generation and detection. One year later, he involved in a project of the Dutch National Technology Funds (STW-EOE5440) as a Postdoctoral Researcher with the Eindhoven University of Technology, The Netherlands, where he studied the semiconductor photonic devices based on the integrated optics. Until October 2003, he was with Capital Normal University, Beijing, where he worked on THz spectroscopy and imaging. In January 2004, he was appointed as a Full Professor at Capital Normal University. He was responsible for 16 projects on the aspects of THz generation, detection, functional materials, and components and its application in the field of THz spectroscopy and THz imaging. He is currently working on THz functional materials and its devices, including THz metamaterials and metasurfaces devices. He is also working on THz technology, THz photonic functional materials, and THz devices. He is also the Vice Group Leader of the Beijing Key Laboratory for THz Spectroscopy and Imaging. He has published over 100 articles on some important journals. In recent years, he was appointed as an invitation reviewer for several journals. He is also a Senior Member of the Chinese Optical Society, the Chinese Physics Society, and the Chinese Society on Analysis and Testing.

SHUQIN LOU received the Ph.D. degree from Beijing Jiaotong University, Beijing, China, in 2005. She is currently a Professor with the School of Electronic and Information Engineering, Beijing Jiaotong University. She has authored or coauthored more than 200 articles on international journals, including *Optics Express*, IEEE Photonics Technology Letters, and IEEE/OSA Journal of Lightwave Technology. Her current research interests include the microstructured fiber, fiber components, fiber laser, and fiber sensor

SHUAI YANG was born in Beijing, China, in 1989. He received the B.S. degree from the Nanjing University of Science and Technology, Nanjing, China, in 2012. He is currently pursuing the Ph.D. degree in optics with the School of Science, Beijing Jiaotong University, Beijing. His current research interests include hollow core anti-resonant fiber and terahertz waveguide.

JIAOYAN GUO was born in Shanxi, China, in 1995. She received the B.S. degree from Xinzhou Normal University, in 2018. She is currently pursuing the master's degree in condensed matter physics with Capital Normal University. Her current research interests include terahertz spectrum and terahertz vortex beam.

• • •